small
NANO MICRO
www.small-journal.com

Biosynthesis and Characterization of Copper Nanoparticles Using *Shewanella oneidensis*: Application for Click Chemistry

Richard L. Kimber, Edward A. Lewis, Fabio Parmeggiani, Kurt Smith, Heath Bagshaw, Toby Starborg, Nimisha Joshi, Adriana I. Figueroa, Gerrit van der Laan, Giannantonio Cibin, Diego Gianolio, Sarah J. Haigh, Richard A. D. Pattrick, Nicholas J. Turner, and Jonathan R. Lloyd**

Copper nanoparticles (Cu-NPs) have a wide range of applications as heterogeneous catalysts. In this study, a novel green biosynthesis route for producing Cu-NPs using the metal-reducing bacterium, *Shewanella oneidensis* is demonstrated. Thin section transmission electron microscopy shows that the Cu-NPs are predominantly intracellular and present in a typical size range of 20–40 nm. Serial block-face scanning electron microscopy demonstrates the Cu-NPs are well-dispersed across the 3D structure of the cells. X-ray absorption near-edge spectroscopy and extended X-ray absorption fine-structure spectroscopy analysis show the nanoparticles are Cu(0), however, atomic resolution images and electron energy loss spectroscopy suggest partial oxidation of the surface layer to Cu_2O upon exposure to air. The catalytic activity of the Cu-NPs is demonstrated in an archetypal "click chemistry" reaction, generating good yields during azide-alkyne cycloadditions, most likely catalyzed by the Cu(I) surface layer of the nanoparticles. Furthermore, cytochrome deletion mutants suggest a novel metal reduction system is involved in enzymatic Cu(II) reduction and Cu-NP synthesis, which is not dependent on the Mtr pathway commonly used to reduce other high oxidation state metals in this bacterium. This work demonstrates a novel, simple, green biosynthesis method for producing efficient copper nanoparticle catalysts.

1. Introduction

Due to its high natural abundance and relatively low cost, copper has attracted considerable attention as a viable alternative to more traditional rare and expensive precious metal catalysts. Copper nanoparticles (Cu-NPs) have a wide range of applications in organic transformations, gas-phase catalysis, photocatalysis, and electrocatalysis.[1] Particularly, copper catalysis has attracted significant interest since the discovery that the Huisgen 1,3-dipolar cycloaddition reaction of azides with terminal alkynes can be greatly accelerated in the presence of copper(I) under mild conditions, combined with high regioselectivity toward the 1,4-disubstituted 1,2,3-triazole.[2,3] Copper-catalyzed azide-alkyne cycloaddition (CuAAC) is an archetypal "click chemistry" reaction and has a wide range of applications in drug discovery,[4–6] bioconjugation,[7–9] and materials science.[8,10]

Dr. R. L. Kimber, Dr. K. Smith, Dr. H. Bagshaw, Dr. N. Joshi, Prof. R. A. D. Pattrick, Prof. J. R. Lloyd
School of Earth and Environmental Sciences and Williamson Research Centre for Molecular Environmental Science
University of Manchester
Manchester M13 9PL, UK
E-mail: richard.kimber@manchester.ac.uk; jon.lloyd@manchester.ac.uk

Dr. E. A. Lewis, Dr. S. J. Haigh
School of Materials
University of Manchester
Manchester M13 9PL, UK

Dr. F. Parmeggiani, Prof. N. J. Turner
School of Chemistry
Manchester Institute of Biotechnology
University of Manchester
Manchester M1 7DN, UK

The ORCID identification number(s) for the author(s) of this article can be found under https://doi.org/10.1002/smll.201703145.

DOI: 10.1002/smll.201703145

Dr. T. Starborg
Wellcome Centre for Cell Matrix Research
University of Manchester
Manchester M13 9PT, UK

Dr. A. I. Figueroa, Prof. G. van der Laan
Magnetic Spectroscopy Group
Diamond Light Source
Didcot, Oxfordshire OX11 0DE, UK

Dr. G. Cibin, Dr. D. Gianolio
Diamond Light Source
Didcot, Oxfordshire OX11 0DE, UK

Nanoparticles make excellent catalysts due to their high surface area and increased number of defect sites relative to polycrystalline materials.[11,12] Furthermore, the use of heterogeneous catalysts such as Cu-NPs offers advantages in increased reusability and efficiency, compared to their homogeneous counterparts.[13,14] Microbial metabolism can be harnessed to offer potentially simple, inexpensive, environmentally benign processes for nanocatalyst production.[15] Proteins and other biomolecules involved in the microbial process can act as capping agents, enhancing nanoparticle stability and limiting aggregation, thus preventing the need for chemical capping agents or surfactants.[16] In addition, the process can be scaled-up and controlled to produce nanoparticles with highly tuned properties.[17,18]

Shewanella oneidensis is one of the most versatile and well-studied species of metal-reducing bacteria, able to reduce a wide range of metals under anaerobic conditions via direct electron transfer linked to respiratory processes,[19] precipitating extracellular or intracellular metallic nanoparticles such as U, Se, Pd, Au, and Ag.[15,20–23] However, to our knowledge, there have been no studies on the synthesis of Cu-NPs by metal-reducing bacteria, including *Shewanella* species. Microbial synthesis of extracellular Cu-NPs was shown to be facilitated by the Cu-resistant intestinal commensal bacterium, *Morganella morganii*, by Ramanathan et al.,[24] but the reduction methods in this organism remain poorly understood and only limited characterization of the Cu-NPs was performed. Furthermore, the catalytic activity of Cu-NPs synthesized by any microbial process remains to be tested.

This is the first study to investigate bioreduction of Cu(II) and synthesis of Cu-NPs using anaerobic metal-reducing bacteria, which are known to have potential for the production of a wide range of catalytically active metallic nanoparticles.[15] *S. oneidensis* MR-1 was selected for study given the broad range of metals that it can reduce, and the availability of deletion mutants that can provide insights into the potential mechanisms of electron transfer to Cu(II), and the formation of reduced Cu-NPs. The Cu-NPs produced by this organism were characterized using a wide range of analytical techniques including transmission electron microscopy (TEM), X-ray absorption near-edge spectroscopy (XANES), extended X-ray absorption fine-structure spectroscopy (EXAFS), electron energy loss spectroscopy (EELS) and a novel technique for 3D imaging of biomass supported nanoparticles, serial block-face scanning electron microscopy (SBFSEM). Finally, the catalytic potential of biogenic Cu-NPs formed by *S. oneidensis* was demonstrated for the synthesis of a series of 1,2,3-triazole derivatives through azide-alkyne cycloadditions, representative of commercially important "click chemistry" reactions.

2. Results and Discussion

2.1. Formation and Characterization of Cu-NPs

To optimize Cu-NP production, cell viability was assessed at a range of Cu(II) concentrations (Figure S1, Supporting Information). After 24 h, growth in the presence of 10×10^{-6} M Cu(II) was equal to that of the no Cu control. At 100 and 500×10^{-6} M Cu(II), growth after 24 h was 20% and 0%, respectively, compared to the no Cu control. Based on these data, a concentration of 50×10^{-6} M Cu(II) was chosen for the bioreduction experiments. To produce biogenic Cu-NPs, washed cells of the metal-reducing bacterium *S. oneidensis* MR1 were supplied with 50×10^{-6} M Cu(II) ions ($CuSO_4$) and 30×10^{-3} M lactate as the electron donor. After 3 h, 70% of Cu was removed from solution (Figure S2, Supporting Information), concurrent with a color change of the solution from colorless to pink indicating bioreduction of Cu(II). After 24 h, 91% removal of Cu from solution was observed followed by complete removal (100%) after 96 h (data not shown). Whole mount TEM images revealed that Cu(II) bioreduction resulted in the formation of Cu-NPs (Figure S3, Supporting Information). TEM images of thin sections of the cells showed the majority of the Cu-NPs were precipitated intracellularly, although precipitates can also be seen in the extracellular matrix, sometimes forming larger agglomerates associated with the outer membrane of the cells (**Figure 1**a–d). Energy dispersive X-ray (EDX) point analysis performed during TEM imaging (Figure S4, Supporting Information) and EDX spectrum imaging performed in the scanning transmission electron microscope (STEM) (Figure 1f) confirms the electron dense precipitates observed in the thin sections are Cu rich. The intracellular precipitates were found within both the periplasm and cytoplasm, as shown in Figure 1. Analysis of the size distribution of the nanoparticles, based on measurements of 80 randomly selected particles, shows the majority (88%) are present in the range of 20–50 nm (Figure S5, Supporting Information). A small number (5%) of larger aggregates above 200 nm are also present. As can be seen in Figure 1, the majority of the smaller particles are intracellular whereas the larger agglomerates tend to be associated with the outer membrane of the cells.

The location of the Cu-NPs was further determined using a novel technique for imaging biomass supported nanoparticles; SBFSEM. The dispersion of the Cu-NPs on the 3D structure of individual cells is shown (**Figure 2**). The 3D electron images, combined with the TEM–EDX and STEM–EDX data from the same sample, confirm that the Cu-NPs are predominately intracellular and that these precipitates typically fall within the smaller (20–50 nm) size range (Figure 2).These images also confirm the larger particles, generally larger than 50 nm, are located in the extracellular matrix. The dispersion of NPs is an important factor affecting their catalytic activity and the 3D electron images also clearly show the Cu-NPs are very well dispersed across the cell structure, which acts as the support matrix for the NPs. In addition, the spherical 3D shape of the Cu-NPs can be seen clearly as well as the volume fraction of the nanoparticles on the biomass support. This highlights the ability of *S. oneidensis* to both synthesize and support Cu-NPs under environmentally benign conditions without the need of chemical reductants or treatments.

XANES of the Cu-NPs was carried out at the Diamond Light Source to characterize the valence and local structure of the nanoparticles. XANES collected at the Cu *K*-edge of the Cu-NPs had an absorption edge located at 8979.3 eV. The absorption edges of the Cu foil, Cu_2O,

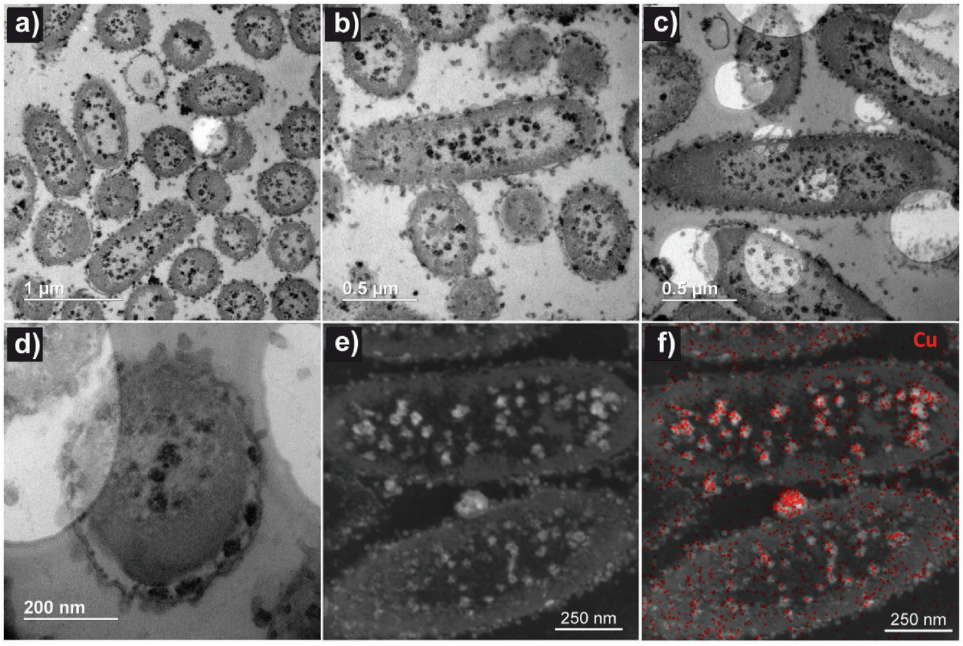

Figure 1. a–d) Thin section TEM images of *Shewanella oneidensis* MR-1 and copper nanoparticles. e) High-angle annular dark field (HAADF) image and f) Cu EDX map performed at the Cu *Kα* peak.

and CuO references were located at 8979.3, 8980.6, and 8983.7 eV, respectively. The excellent match between the spectra for Cu foil and the Cu-NPs clearly demonstrates that the bioreduction process involved reduction of Cu(II) to Cu(0) (**Figure 3**a). When collected at the Cu $L_{2,3}$-edges, XANES spectra from the Cu-NPs also showed an excellent match to the Cu foil reference (Figure 3b), providing further evidence of the bioreduction of Cu(II) to Cu(0). No peaks suggestive of oxidation to Cu(I) or Cu(II) were observed at either the Cu *K*-edge or Cu $L_{2,3}$-edges. On the other hand, spectra collected at the Cu $L_{2,3}$-edges from commercial Cu(0) particles showed a peak at ≈931 eV, indicative of Cu(II) and a strong peak at ≈933 eV, indicative of Cu(I), suggesting the biogenic Cu-NPs are more stable against oxidation than commercially available Cu(0) particles, possibly due to the presence of capping proteins/peptides associated with bacterially produced nanoparticles.[16]

Given the data obtained from the XANES analysis, EXAFS data were fitted assuming a similar coordination environment as cubic Cu(0) (Figure 3c,d).[25] The best fit was obtained with Cu coordinated by 9.6 Cu atoms at 2.54 ± 0.02 Å, 6 Cu atoms at 3.57 ± 0.04 Å, 24 Cu atoms at 4.45 ± 0.03 Å, and 9 Cu atoms at 5.29 ± 0.18 Å. See Table S1 in the Supporting Information for complete details of fit. The fit was broadly consistent with the reference structure. However, 9.6 and 9 Cu atoms were determined to be coordinated at 2.54 and 5.29 Å, respectively; slightly lower than noted in the ideal structure of 12 Cu atoms in both shells. It is possible that this reduced coordination is caused by the nanoparticulate nature of the materials in this study.[26]

Polycrystalline select area electron diffraction patterns of the nanoparticle agglomerates further support the X-ray absorption spectroscopy (XAS) analysis that the Cu-NPs exist predominantly as metallic Cu (**Figure 4**a,b). However, lattice fringes and electron diffraction patterns of some of the smallest particles ≤10 nm, are consistent with Cu_2O (Figure 4c). EELS performed on the interior of the particles shows Cu $L_{2,3}$-edge features which match the reference spectrum for Cu(0) (**Figure 5**). However, EELS spectra taken at the edge region of the same particle matches closely with the reference spectrum of Cu_2O. It should be noted that the samples were briefly exposed to air during their transfer into the TEM. Taking together the XAS and EELS data suggests the Cu-NPs are predominantly Cu(0). However,

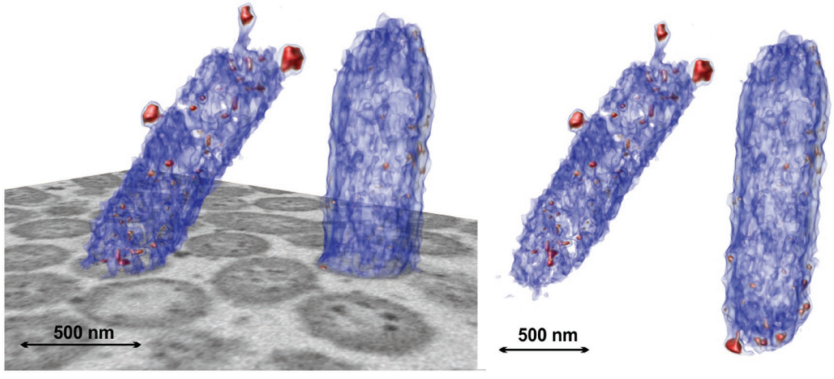

Figure 2. Reconstructed "3D" SBFSEM image showing the dispersion of copper nanoparticles in cells of *Shewanella oneidensis* MR-1. The blue color is applied to the "light" low atomic weight elements of each scan and represents the cellular structure. The red is applied to the "dark" heavier elements of the SEM scans and represents the Cu nanoparticle component.

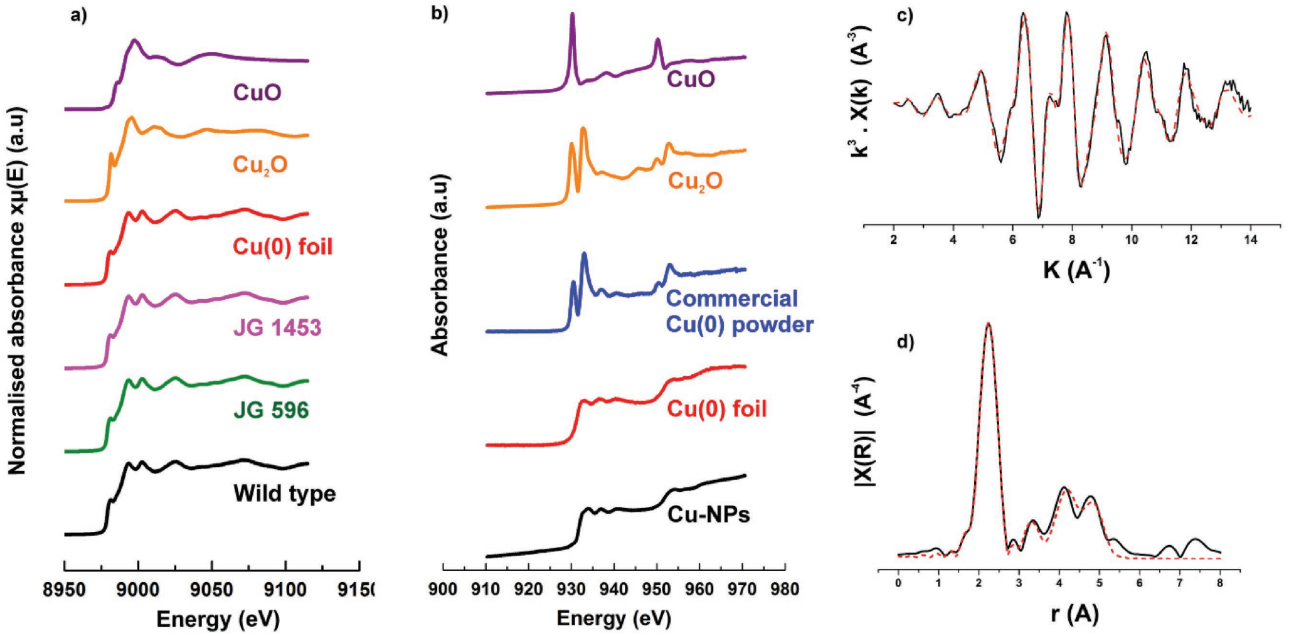

Figure 3. a) XANES for the Cu *K*-edge of Cu-NPs produced by cells of *S. oneidensis* MR-1 (wild type) and cytochrome deletion mutants and b) Cu $L_{2,3}$-edge of the Cu-NPs produced by the wild type. c) EXAFS and d) corresponding Fourier transform for the Cu *K*-edge of the Cu-NPs. Data are shown by the black (solid) line and the fit is shown by the red (dotted) line.

a thin Cu_2O shell may develop at the surface layer of the particles upon exposure to air, while the core of the particles remain stable as Cu(0). Mansour et al. also observed the formation of a Cu_2O shell around chemically synthesized Cu(0) nanoparticles under an oxygen atmosphere.[27]

2.2. Application in the Cu(I)-Catalyzed Azide-Alkyne Cycloaddition

To test the catalytic activity of the Cu-NPs, we investigated the synthesis of a range of triazole derivatives via the Cu(I)-catalyzed cycloaddition of benzyl azide **(1)**, with a representative panel of alkynes **(2a–c)** (**Scheme 1**). Under mild reaction conditions, with no further processing of the biogenic Cu-NPs, complete conversions (as monitored by ^{1}H NMR) were obtained using a relatively low catalyst loading of 1.1 mol%. As expected, all reactions showed complete regioselectivity toward 1,4-disubstituted triazoles. Although Cu(0) has been used to carry out CuAAC,[28] the reaction is accepted to be catalyzed by Cu(I) species at the nanoparticle surface.[29,30] Our XANES and EXAFS analysis indicate the formation of Cu(0) nanoparticles, however,

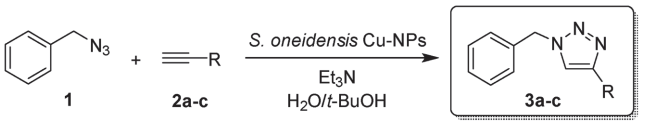

a: R=Ph (66%)
b: R=*n*-Bu (79%)
c: R=*p*-MeOC$_6$H$_4$ (51%)

Scheme 1. Synthesis of substituted triazoles mediated by *S. oneidensis* Cu-NPs.

atomic resolution images and EELS analysis suggest a thin Cu_2O shell is present after exposure to air and hence, this Cu(I) surface layer is likely responsible for the CuAAC activity of the biosynthesized nanoparticles. The inherent nature of

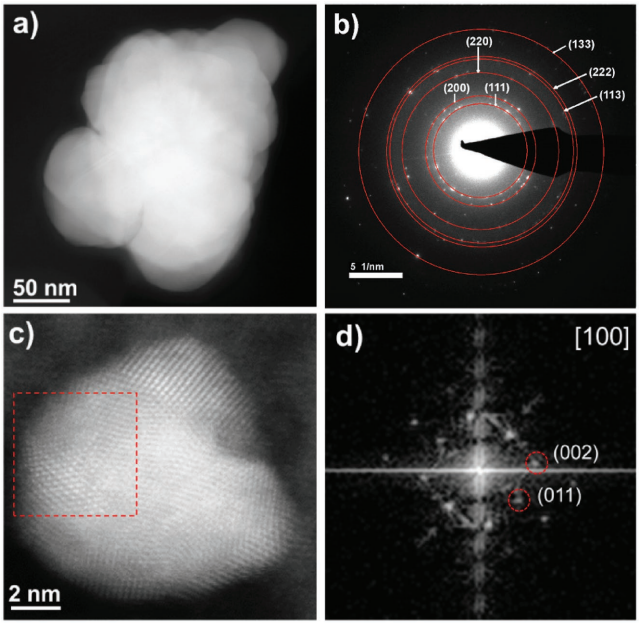

Figure 4. a) HAADF STEM image of agglomerated biogenic copper nanoparticles with b) corresponding polycrystalline select area diffraction pattern which corresponds to the FCC crystal structure of Cu(0). c) Atomic resolution HAADF STEM image of small nanocrystal (≈10 nm diameter), the Fourier transform (FT) taken from the region indicated by the dashed box in (c) is shown in (d) and indexes to Cu_2O viewed down the [100] zone axis.

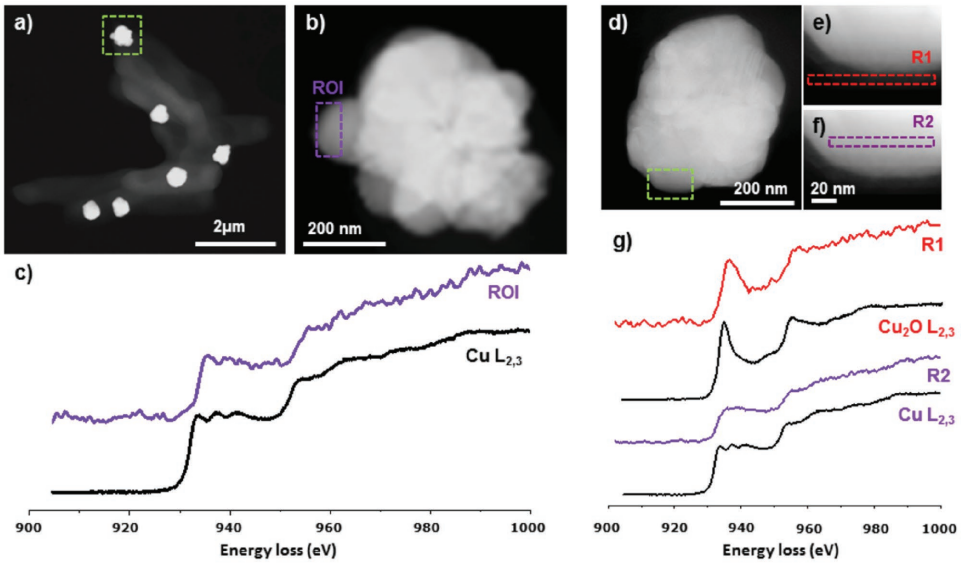

Figure 5. a) HAADF image of cells of *S. oneidensis* MR-1 and Cu-NPs. Cu-NPs selected for EELS analysis are highlighted in the dashed (green) box in (a) and are shown in (b). c) EELS spectrum of the region of interest (ROI) from image (b) (purple line) compared to reference spectrum of Cu metal (black line). d) HAADF image of Cu-NPs; the region analyzed in (e) and (f) is indicated by a dashed (green) box in (d). e) Region of interest at edge of the particle (R1); f) region of interest representing the bulk particle (R2); g) corresponding EELS spectra from the two regions of interests highlighted in images (e) (red line) and (f) (purple line) compared to reference spectra of Cu_2O and Cu metal (black lines).

nanoparticles to agglomerate and oxidize further often requires inorganic supports or stabilizing agents to maintain good catalytic activity.[31] Here, no additional supporting or stabilizing agents were required and no steps were taken to separate the nanoparticles from the biomass demonstrating a simple, green, and effective method for producing catalytically active Cu-NPs. Although good isolated yields (51–79%) were reported here, further work to optimize the system is important, for example, to determine optimal reaction times and Cu-NP catalyst loading to improve yields.

2.3. Mechanistic Insights into Cu(II) Bioreduction and Nanoparticle Formation

In order to develop the mechanistic understanding of Cu-NP biosynthesis by *S. oneidensis*, we compared Cu(II) bioreduction using the wild type strain and two deletion mutants. Metal reduction in *S. oneidensis*, and in other metal-reducing bacteria, is often facilitated by a network of periplasmic and/or outer membrane *c*-type cytochromes (heme-containing proteins), which act as terminal reductases for the metals during anaerobic respiration. The Mtr pathway, an electron transport chain containing a series of *c*-type cytochromes which transfer electrons from the cytoplasm to the outer membrane, is one of the key pathways for metal reduction in *S. oneidensis* and has been shown to play an important role in the reduction of poorly soluble Fe(III)- and Mn(IV)-minerals[32–34] as well as soluble U(VI),[20] Tc(VII),[35] and V(V).[36] To identify the importance of various *c*-type cytochromes in Cu(II) bioreduction and Cu-NP formation, bioreduction was compared using *S. oneidensis* MR-1 wild type cells with those of two cytochrome deletion mutants, JG596 and JG1453.

Deletion of the outer membrane *c*-type cytochromes MtrC, MtrF, and OmcA (JG596) and the outer membrane and periplasmic cytochromes MtrABCDEF, OmcA, DmsE, S04360, CctA (JG1453) had little effect on the rate or extent of Cu(II) reduction. When supplied with 50×10^{-6} M Cu(II), the two mutant strains reduced 82–89% of Cu(II) over 24 h, compared to the 91% reduced by the wild type (Figure S2, Supporting Information). All strains reduced 100% Cu(II) after 72 h. When 200×10^{-6} M Cu(II) was used, all 3 strains reduced between 26% and 32% of the Cu after 24 h (Figure S2, Supporting Information). Heat-killed cell controls showed no decrease in Cu(II) solution concentrations (Figure S2, Supporting Information) suggesting that Cu(II) removal was facilitated predominately by active Cu uptake and/or bioreduction by metabolically active cells, rather than by passive biosorption to the cell biomass. TEM images and associated EDX data of cells from both a heat-killed and Cu free control show no presence of any Cu-NPs, providing further support that Cu-NP formation is facilitated by metabolically active cells (Figure S6, Supporting Information). Cell free controls containing the electron donor lactate also showed no Cu(II) removal (Figure S2, Supporting Information), consistent with enzymatic "bioreduction" mechanisms. The morphology and localization of the Cu-NPs produced by the deletion mutants was similar to that seen in the wild type, with small (20–40 nm) individual particles being the most dominant and some larger agglomerates also present. The similarity in both extent and rate of reduction between the wild type and mutants suggests that Cu(II) reduction is not facilitated by direct contact with *c*-type cytochromes in the Mtr pathway (beyond the cytoplasmic membrane-bound cytochrome CymA).The similarity in Cu-NP precipitation and morphology between the wild type and deletion mutants further supports this.

Deletion of MtrC and OmcA has also been shown to have little impact on the reduction of Pd(II) and Se(IV).[37,38] Deletion of hydA which encodes the [NiFe]-hydrogenase HyaB significantly slowed the bioreduction of Pd(II), whereas a mutant lacking the fumarate reductase FccA showed significantly decreased Se(IV) reduction capability. NADH dehydrogenase-2 (NDH-2) was shown to promote Cu(II) reduction to Cu(I) under aerobic conditions in *Escherichia coli*.[39] NDH-2 is present as a cytoplasmic membrane-bound enzyme, upstream of CymA, in *S. oneidensis* and so may play a role in Cu(II) reduction coupled to NADH oxidation. Therefore, the diverse electron transport pathways in *S. oneidensis* present a wide range of possible mechanisms outside of the Mtr pathway, which could facilitate Cu(II) reduction. Further work is required to identify the specific reductase(s) responsible.

The observation of substantial cytoplasmic Cu-NP precipitation (Figures 1 and 2) is surprising as for most bacteria, copper-requiring enzymes are located either within the periplasm or embedded in the cytoplasmic membrane, and so there are no known metabolic requirements for copper to enter the cytosol.[40] Hence, a variety of Cu defense mechanisms, including cytoplasmic Cu exporters,[41] tightly control Cu homeostasis in Gram-negative bacteria including *S. oneidensis*. We suggest several mechanisms which may be responsible for the extent of Cu-NPs observed in the periplasm and cytoplasm: (i) Cu(II) ions were able to enter the periplasm and cytoplasm where an, as yet, unidentified reductase/s reduced and precipitated the Cu-NPs; (ii) reduction of Cu(II) and precipitation of the Cu-NPs in the periplasm or cytoplasm followed by transport of the reduced NPs across the cytoplasmic membrane, possibly facilitated by membrane damage caused by Cu toxicity; (iii) reduction of Cu(II) to Cu(I) in the cytoplasm followed by Cu(I) export and subsequent disproportionation to form Cu(0) and Cu(II). The later was suggested by Hofacker et al. and Weber et al. as the mechanism responsible for Cu(0) formation by bacteria under soil reducing conditions.[42,43] However, they were unable to replicate Cu(0) formation in cell suspensions of *Clostridium* species implicated in this study.

3. Conclusions

This study demonstrates the ability of *S. oneidensis* to facilitate the bioreduction of Cu(II) to form well-dispersed, biomass supported Cu(0) nanoparticles under environmentally benign conditions. Deletion mutants indicate that the Mtr pathway does not play an important role in the reduction process and suggest a novel reductase/s may be involved. Detailed characterization reveals the majority of nanoparticles are located within the periplasm and cytoplasm, further suggesting that bioreduction is an intracellular process. The nanoparticles remain stable against oxidation under anaerobic conditions, however, EELS spectra and atomic resolution high-angle annular dark field (HAADF) STEM images suggest that, when exposed to air, a partially oxidized Cu_2O thin shell develops. The Cu-NPs display good catalytic activity toward copper catalyzed azide-alkyne cycloaddition demonstrating a simple and green synthesis method for producing reactive Cu nanocatalysts. The possibility of targeting Cu(II) in wastewaters via bioreduction offers the potential to revalorize a range of industrial effluents e.g. from mining activities, adding an extra financial incentive to evaluate this emerging technology.

4. Experimental Section

Shewanella oneidensis: All cultures of *S. oneidensis* were grown anaerobically in a fully defined, presterilized, liquid minimal medium (pH 7.4) based on that described previously by Myers and Nealson:[44] 9×10^{-3} M $(NH_4)_2SO_4$; 5.7×10^{-3} M K_2HPO_4; 3.3×10^{-3} M KH_2PO_4; 2.2×10^{-3} M $NaHCO_3$; 1×10^{-3} M $MgSO_4 \cdot 7H_2O$; 0.49×10^{-3} M $CaCl_2 \cdot 2H_2O$; 67.2×10^{-6} M Na_2EDTA; 56.6×10^{-6} M H_3BO_3; 10×10^{-6} M NaCl; 5.4×10^{-6} M $FeSO_4 \cdot 7H_2O$; 5×10^{-6} M $CoCl_2 \cdot 6H_2O$; 5×10^{-6} M $NiCl_2 \cdot 6H_2O$; 3.9×10^{-6} M $Na_2MoO_4 \cdot 2H_2O$; 1.5×10^{-6} M Na_2SeO_4; 1.3×10^{-6} M $MnCO_3$; 1×10^{-6} M $ZnCl_2$; 0.2×10^{-6} M $CuSO_4 \cdot 5H_2O$; 20 mg L^{-1} L-arginine HCl; 20 mg L^{-1} L-glutamate; 20 mg L^{-1} L-serine; 100×10^{-3} M sodium DL-lactate (carbon source and electron donor); 20×10^{-3} M fumarate (electron acceptor). Serum bottles (100 mL) containing the defined medium were flushed with an 80:20 gas mix of N_2:CO_2 for 20 min to remove O_2 and then sealed and autoclaved to sterilize the medium. After cooling, the medium was inoculated with a late log/early stationary phase culture to give an optical density of 0.02 at 600 nm. The cultures were grown for 24 h at 30 °C. The fully grown cultures were transferred anaerobically to centrifuge tubes, and the cells pelleted by centrifugation at 4960 rpm for 20 min at 4 °C. The cells were washed two times with fresh anoxic, sterilized 3-(N-morpholino)propanesulfonic acid (MOPS) buffer and then were resuspended in the same buffer at pH 7.1.

Cytochrome-Deletion Mutants: The *c*-type cytochrome deletion mutant JG596 lacks the outer membrane cytochromes MtrC, MtrF, and OmcA[45] where as JG1453 lacks the all the important cytochromes beyond the cytoplasmic membrane-bound tetrahaem *c*-type cytochrome CymA, namely: MtrABCDEF, OmcA, DmsE, S04360, CctA.[46] The mutants were cultured as described above for the MR-1 wild type strain. Both mutant strains were kindly provided by Jeff Gralnick (University of Minnesota).

Copper Bioreduction: The kinetics and extent of copper reduction by *S. oneidensis* MR-1 wild type and mutants was determined using a standard resting cell experiment. The copper reduction assay contained Cu(II) supplied as $CuSO_4$ (50×10^{-6} M or 200×10^{-6} M) and sodium lactate (30×10^{-3} M) as the electron donor in MOPS buffer (30×10^{-3} M) adjusted to pH 7.1. The medium was purged with an 80:20 gas mix of N_2:CO_2 for 20 min to remove O_2, sealed with thick butyl rubber stoppers and autoclaved. Late log/early stationary phase cells were washed and harvested and then added aseptically to achieve a final optical density of 0.1 and incubation was carried out at 20 °C. Soluble Cu(II) was determined by taking aliquots and centrifuging at 14 900 rpm for 10 min to pellet the cells and insoluble copper. Samples were taken from the supernatant and Cu(II) in solution measured using inductively coupled plasma atomic emission spectroscopy (ICP-AES).

Serial Block-Face Scanning Electron Microscopy (3View): 1 mL suspensions of wild type *S. oneidensis* MR-1 challenged with Cu(II) (50×10^{-6} M), with sodium lactate (30×10^{-3} M) as the electron donor, were taken and centrifuged at 14 900 rpm for 10 min. The supernatant was discarded and the cells were resuspended and washed in anoxic deionized water. The cell suspension was centrifuged again, the resulting pellet was fixed in glutaraldehyde (2.5%), Paraformaldehyde (4%) in HEPES (0.1 M, pH 7.2) for 1 h at room temperature. Following the initial fixation the pellet was resuspended in low melting point agarose (1.5%), spun down and set on ice. The pellet was cut to size and fixed in primary fix for a further hour at room temperature. Following this it was treated as a solid tissue sample and taken for a standard TEM preparation. Briefly, it was washed three times in deionized water for 5 min on a rotary shaker. Reduced osmium (1% osmium with 0.75% potassium ferrocyanide in 0.1 M sodium cacodylate buffer pH 7.2) was added as a secondary fix/stain and the pellet was then washed five times as before. Uranyl acetate was added as a further stain before another two washes were performed. The pellet was then dehydrated for 15 min in increasing ethanol solutions

(30%, 50%, 70%, 90%, 100%) before being washed twice in acetone for 30 min. The resin was infiltrated using increasing concentrations (25%, 50%, 75%, 100%) with each infiltration alternating over night or over a day. Finally, the pellet was put into molds with fresh resin and set in an oven at 60 °C for 2 d. Serial block face image stacks were collected using a Gatan 3view mounted in an FEI Quanta 250FEG. The microscope was run at 0.3 Torr, 3.8 kV. Images (4096 × 4096) were collected with 5.58 nm pixels, with a 1 µs dwell time with slices cut at 50 nm.

TEM and STEM Imaging and EELS of Whole Mount Samples: Whole mount TEM samples of cultures of the wild type MR-1 and mutants were prepared in an anaerobic chamber using anoxic solutions. 1 mL of cell suspensions of *S. oneidensis* MR-1 challenged with Cu(II) (50×10^{-6} M) with sodium lactate (30×10^{-3} M) were taken after 24 h and centrifuged at 14 900 rpm for 5 min, the supernatant discarded and the pellet resuspended in 1 mL deionized water. The cell suspension (1.5 µL) was pipetted onto a gold TEM grid with a holey-carbon or carbon-coated formvar support film and allowed to air dry in an anaerobic chamber. Samples were kept anaerobic until they were transferred into the TEM chamber, during which they would have been very briefly exposed to the atmosphere. TEM imaging and EDX analysis were performed in an FEI Tecnai F30 FEG Analytical TEM operated at 300 kV. EDX analysis was performed with the sample tilted at the optimum angle toward the detector to increase collection efficiency.

STEM imaging, EDX analysis, and EELS of whole mount samples were performed in a probe side aberration-corrected FEI Titan G2 with an X-FEG electron source operated at 200 kV. High angle annular dark field (HAADF) STEM imaging was performed using a probe convergence angle of 21 mrad, a HAADF inner angle of 54 mrad, and a probe current of ≈180 pA. EELS was performed using a Gatan Imaging Filter Quantum ER system with a 5×10^{-3} M entrance aperture, a collection angle of 62 mrad and an energy dispersion of 1 eV. EDX analysis was performed using a Super-X four silicon drift EDX detector system with a total collection solid angle of 0.7 srad, all four detectors were turned on and the sample was not tilted.

TEM and STEM Imaging of Thin Section Samples: Cross-section TEM and STEM samples of cultures of the MR-1 wild type strain were prepared from the 3view pins. Sections (50–70 nm) were cut with a diamond knife on a Reichert-Jung Ultracut. The sections were collected onto holey-carbon supported gold TEM grids. Thin section TEM and EDX analysis were performed in an FEI Tecnai F30 FEG Analytical TEM operated at 300 kV as described above. Thin section STEM and EDX analysis were performed using an Oxford Instruments X-Max silicon drift EDX detector system with data collection and analysis performed using Oxford Instruments Aztec software suite.

XAS Characterization: For XAS characterization at the Cu *K*-edge, 1 mL aliquots of *S. oneidensis* MR-1 challenged with Cu(II) (50×10^{-6} M) and sodium lactate (30×10^{-3} M) were taken and centrifuged (14 900 rpm for 5 min), the supernatant discarded and the pellet resuspended in 1 mL anoxic deionized water. 200 µL of the suspension was pipetted onto a plastic weighing boat and air dried overnight. All manipulations were performed inside an anaerobic chamber. Samples were mounted onto a layer of kapton tape which in turn was mounted onto an aluminum sample holder. A further layer of kapton tape was applied over the samples to maintain anaerobicity. EXAFS spectra were collected at room temperature at the Cu *K*-edge (≈8980 eV) on beamline B18 at the Diamond Light Source. A 36-element solid-state Ge detector with digital signal processing for fluorescence EXAFS, high energy resolution, and high count rate was used to measure with the beam at 45° incidence with respect to the sample holder plane. All spectra were acquired in quick-EXAFS mode, using the Pt-coated branch of collimating and focusing mirrors, a Si(111) double-crystal monochromator and a pair of harmonic rejection mirrors. XANES processing was carried out using Athena while EXAFS data were modelled using Artemis (Demeter; 0.9.24).[47] Fitting was calculated using multiple k-weights (k1, k2, and k3) and the best fit was calculated in R space by minimization of the reduced X^2. At no point did parameterization of the EXAFS model use more than two-thirds of the total number of available independent points.

For XAS characterization at the Cu $L_{2,3}$-edges, samples were washed as above and then pipetted onto carbon tape mounted on an aluminum sample holder which was sealed in an air-tight coffin to maintain anaerobicity. The samples were loaded into the portable octupole magnet system on beamline I10 at the Diamond Light Source, under a backflow of nitrogen and then held in a vacuum for the duration of the measurement. The XAS spectra were recorded simultaneously using the total electron yield and fluorescence yield detection at room temperature at the Cu $L_{2,3}$-edges.

Synthesis of Triazole Derivatives: Benzyl azide **1** (0.25 mmol, 37 mg), the suitable alkyne **2a–c** (0.25 mmol, 21–33 mg) and Et_3N (0.25 mmol, 25 mg) were dissolved in H_2O/*t*-BuOH (5.0 mL, 8:2). Following bioreduction of Cu(II) (50×10^{-6} M), suspension of *S. oneidensis* cells with associated Cu-NPs were washed three times and then resuspended in deionized water. An aliquot of the suspension (500 µL, equivalent to 1.1 mol% Cu), was added to the solution and the mixture was stirred at room temperature for 12 h. The mixture was extracted with EtOAc (3 × 10 mL), then the combined organic phase was washed with brine (20 mL), dried over anhydrous $MgSO_4$ and evaporated under reduced pressure. The crude product **3a–c** (of sufficient purity for further chemical transformations) was purified either by recrystallization ($EtOH/H_2O$) or by column chromatography on silica (*n*-Hex/EtOAc 8:2). Full characterization of the products is reported in the Supporting Information.

Supporting Information

Supporting Information is available from the Wiley Online Library or from the author.

Acknowledgements

The authors would like to thank NERC for funding under the Resource Recovery from Waste program (NE/L014203/1), and also acknowledges support from from the BBSRC (grants BB/L013711/1 and BB/R010412/1). The authors would also like to thank J. Gralnick (University of Minnesota) for kindly supplying the deletion mutant strains and P. Lythgoe (University of Manchester) for ICP-AES analysis. K.S. would like to acknowledge EnviroRadNet for funding. The authors acknowledge beamtime awarded at the Diamond Light Source for XAS on beamline I10 under proposal SI-15476 and for XANES and EXAFS on beamline B18 under proposal SP-16136.

Conflict of Interest

The authors declare no conflict of interest.

Keywords

biosynthesis, click chemistry, copper nanoparticles, *Shewanella oneidensis*, XANES

Received: September 11, 2017
Revised: November 23, 2017
Published online:

[1] M. B. Gawande, A. Goswami, F. X. Felpin, T. Asefa, X. Huang, R. Silva, X. Zou, R. Zboril, R. S. Varma, *Chem. Rev.* **2016**, *116*, 3722.
[2] V. V. Rostovtsev, L. G. Green, V. V. Fokin, K. B. Sharpless, *Angew. Chem., Int. Ed.* **2002**, *41*, 2596.
[3] C. W. Tornøe, C. Christensen, M. Meldal, *J. Org. Chem.* **2002**, *67*, 3057.

[4] S. G. Agalave, S. R. Maujan, V. S. Pore, *Chem.—Asian J.* **2011**, *6*, 2696.
[5] H. C. Kolb, K. B. Sharpless, *Drug Discovery Today* **2003**, *8*, 1128.
[6] K. B. Sharpless, R. Manetsch, *Expert Opin. Drug Discovery* **2006**, *1*, 525.
[7] T. Zheng, S. H. Rouhanifard, A. S. Jalloh, P. Wu, *Top. Heterocycl. Chem.* **2012**, *28*, 163.
[8] J. E. Moses, A. D. Moorhouse, *Chem. Soc. Rev.* **2007**, *36*, 1249.
[9] R. Breinbauer, M. Köhn, *ChemBioChem* **2003**, *4*, 1147.
[10] W. Xi, T. F. Scott, C. J. Kloxin, C. N. Bowman, *Adv. Funct. Mater.* **2014**, *24*, 2572.
[11] R. Kortlever, J. Shen, K. J. P. Schouten, F. Calle-Vallejo, M. T. M. Koper, *J. Phys. Chem. Lett.* **2015**, *6*, 4073.
[12] A. T. Bell, *Science* **2003**, *299*, 1688.
[13] T. Jin, M. Yan, Y. Yamamoto, *ChemCatChem* **2012**, *4*, 1217.
[14] R. Hudson, C. J. Li, A. Moores, *Green Chem.* **2012**, *14*, 622.
[15] J. R. Lloyd, J. M. Byrne, V. S. Coker, *Curr. Opin. Biotechnol.* **2011**, *22*, 509.
[16] K. B. Narayanan, N. Sakthivel, *Adv. Colloid Interface Sci.* **2010**, *156*, 1.
[17] J. M. Byrne, H. Muhamad Ali, V. S. Coker, J. Cooper, J. R. Lloyd, *J. R. Soc.* **2015**, *12*, 20150240.
[18] J. M. Byrne, N. D. Telling, V. S. Coker, R. A. Pattrick, G. van der Laan, E. Arenholz, F. Tuna, J. R. Lloyd, *Nanotechnology* **2011**, *22*, 455709.
[19] J. R. Lloyd, *FEMS Microbiol. Rev.* **2003**, *27*, 411.
[20] M. J. Marshall, A. S. Beliaev, A. C. Dohnalkova, D. W. Kennedy, L. Shi, Z. Wang, M. I. Boyanov, B. Lai, K. M. Kemner, J. S. McLean, S. B. Reed, D. E. Culley, V. L. Bailey, C. J. Simonson, D. A. Saffarini, M. F. Romine, J. M. Zachara, J. K. Fredrickson, *PLoS Biol.* **2006**, *4*, e268.
[21] C. I. Pearce, R. A. D. Pattrick, N. Law, J. M. Charnock, V. S. Coker, J. W. Fellowes, R. S. Oremland, J. R. Lloyd, *Environ. Technol.* **2009**, *30*, 1313.
[22] W. D. Windt, P. Aelterman, W. Verstraete, *Environ. Microbiol.* **2005**, *7*, 314.
[23] A. K. Suresh, D. A. Pelletier, W. Wang, M. L. Broich, J. W. Moon, B. Gu, D. P. Allison, D. C. Joy, T. J. Phelps, M. J. Doktycz, *Acta Biomater.* **2011**, *7*, 2148.
[24] R. Ramanathan, M. R. Field, A. P. O'Mullane, P. M. Smooker, S. K. Bhargava, V. Bansal, *Nanoscale* **2013**, *5*, 2300.
[25] I. K. Suh, H. Ohta, Y. Waseda, *J. Mater. Sci.* **1988**, *23*, 757.
[26] N. S. Marinković, K. Sasaki, R. R. Adžić, *Zast. Mater.* **2016**, *57*, 101.
[27] M. Mansour, L. Favergeon, M. Pijolat, *Thermochim. Acta* **2013**, *570*, 41.
[28] B. J. Borah, D. Dutta, P. P. Saikia, N. C. Barua, D. K. Dutta, *Green Chem.* **2011**, *13*, 3453.
[29] F. Himo, T. Lovell, R. Hilgraf, V. V. Rostovtsev, L. Noodleman, K. B. Sharpless, V. V. Fokin, *J. Am. Chem. Soc.* **2005**, *127*, 210.
[30] M. R. Decan, S. Impellizzeri, M. L. Marin, J. C. Scaiano, *Nat. Commun.* **2014**, *5*, 4612.
[31] F. Alonso, Y. Moglie, G. Radivoy, *Acc. Chem. Res.* **2015**, *48*, 2516.
[32] L. Shi, T. C. Squier, J. M. Zachara, J. K. Fredrickson, *Mol. Microbiol.* **2007**, *65*, 12.
[33] Y. Xiong, L. Shi, B. Chen, M. U. Mayer, B. H. Lower, Y. Londer, S. Bose, M. F. Hochella, J. K. Fredrickson, T. C. Squier, *J. Am. Chem. Soc.* **2006**, *128*, 13978.
[34] J. K. Fredrickson, J. M. Zachara, *Geobiology* **2008**, *6*, 245.
[35] M. J. Marshall, A. E. Plymale, D. W. Kennedy, L. Shi, Z. Wang, S. B. Reed, A. C. Dohnalkova, C. J. Simonson, C. Liu, D. A. Saffarini, M. F. Romine, J. M. Zachara, A. S. Beliaev, J. K. Fredrickson, *Environ. Microbiol.* **2008**, *10*, 125.
[36] J. M. Myers, W. E. Antholine, C. R. Myers, *Appl. Environ. Microbiol.* **2004**, *70*, 1405.
[37] C. K. Ng, T. K. Cai Tan, H. Song, B. Cao, *RSC Adv.* **2013**, *3*, 22498.
[38] D.-B. Li, Y.-Y. Cheng, C. Wu, W.-W. Li, N. Li, Z.-C. Yang, Z.-H. Tong, H.-Q. Yu, *Sci. Rep.* **2014**, *4*, 3735.
[39] L. Rodríguez-Montelongo, S. I. Volentini, R. N. Farías, E. M. Massa, V. A. Rapisarda, *Arch. Biochem. Biophys.* **2006**, *451*, 1.
[40] S. Tottey, D. R. Harvie, N. J. Robinson, *Acc. Chem. Res.* **2005**, *38*, 775.
[41] A. C. Toes, M. H. Daleke, J. G. Kuenen, G. Muyzer, *Microbiology* **2008**, *154*, 2709.
[42] A. F. Hofacker, S. Behrens, A. Voegelin, R. Kaegi, T. Lösekann-Behrens, A. Kappler, R. Kretzschmar, *Geomicrobiol. J.* **2015**, *32*, 130.
[43] F.-A. Weber, A. Voegelin, R. Kaegi, R. Kretzschmar, *Nat. Geosci.* **2009**, *2*, 267.
[44] C. R. Myers, K. H. Nealson, *Science* **1988**, *240*, 1319.
[45] D. Coursolle, J. A. Gralnick, *Mol. Microbiol.* **2010**, *77*, 995.
[46] D. Coursolle, J. A. Gralnick, *Front. Microbiol.* **2012**, *3*, 56.
[47] B. Ravel, M. Newville, *Phys. Scr.* **2005**, *2005*, 1007.